Electronic Supplementary Material (ESI) for Nanoscale Horizons.

3D Porous FeP/rGO Modulated Separator as Dual-Function Polysulfide Barrier for High-performance Lithium Sulfur Batteries

Yingge Zhang,[a, b, #] Yange Wang,[a, b, #] Rongjie Luo,[a, b, #] Ya Yang,[a, b] Yang Lu,[a, b, *] Yan Guo,[a, b] Xianming Liu,[c] Shixun Cao,[d] Jang-Kyo Kim[e] and Yongsong Luo[a, b, *]

[a]*Key Laboratory of Microelectronics and Energy of Henan Province, Henan Joint International Research Laboratory of New Energy Storage Technology, Xinyang Normal University, Xinyang 464000, P. R. China.*

[b]*School of Physics and Electronic Engineering, Xinyang Normal University, Xinyang 464000, P. R. China.*

[c]*College of Chemistry and Chemical Engineering, Luoyang Normal University, Luoyang 471934, P. R. China.*

[d]*Department of Physics, and International Center of Quantum and Molecular Structures, Materials Genome Institute, Shanghai University, Shanghai 200444, China*

[e]*Department of Mechanical and Aerospace Engineering, Hong Kong University of Science and Technology, Clear Water Bay, Kowloon, Hong Kong, P. R. China.*

[*] To whom correspondence should be addressed: Tel./fax: +86 0376 6390801, E-mail: ysluo@xynu.edu.cn (Y. S. Luo). luyang.181@163.com. [#] These authors contributed equally to this work.

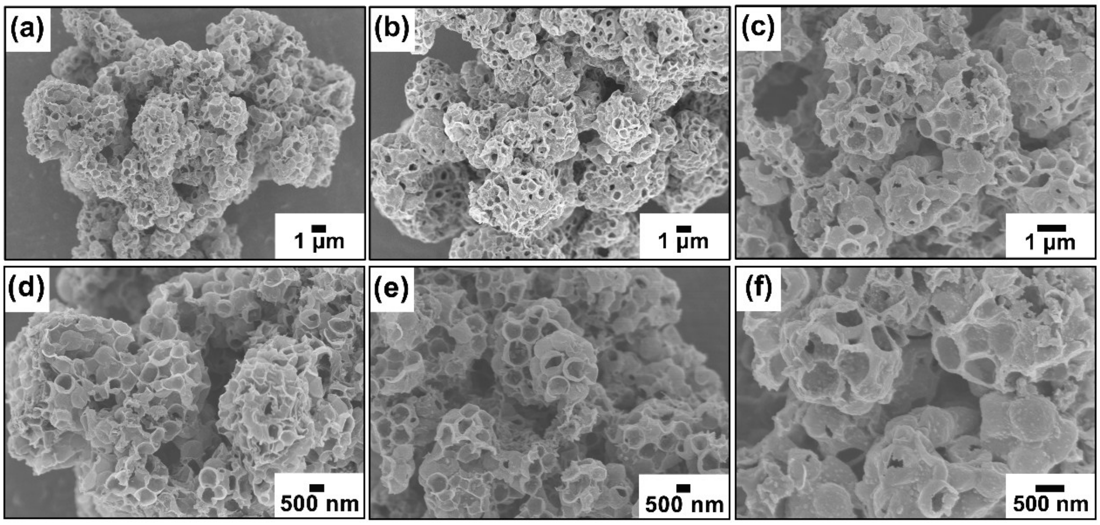

Fig. S1. a) and d) SEM images of FOG microspheres. b) and e) SEM images of FPG microspheres. c) and f) SEM images of FPGS composite.

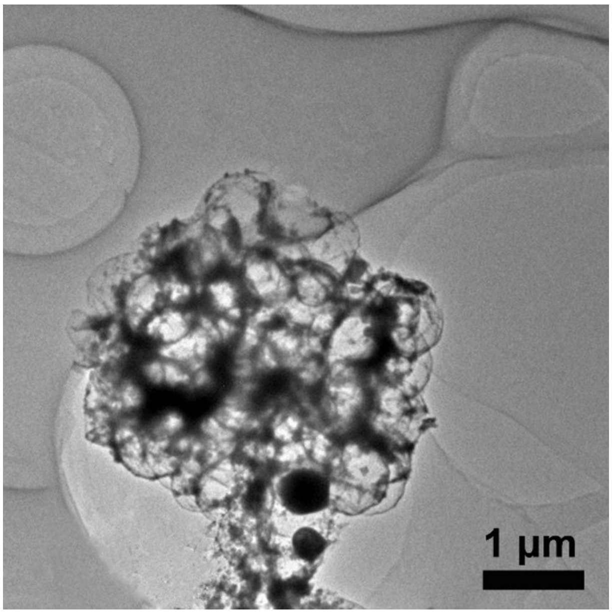

Fig. S2. TEM image of FPG microsphere.

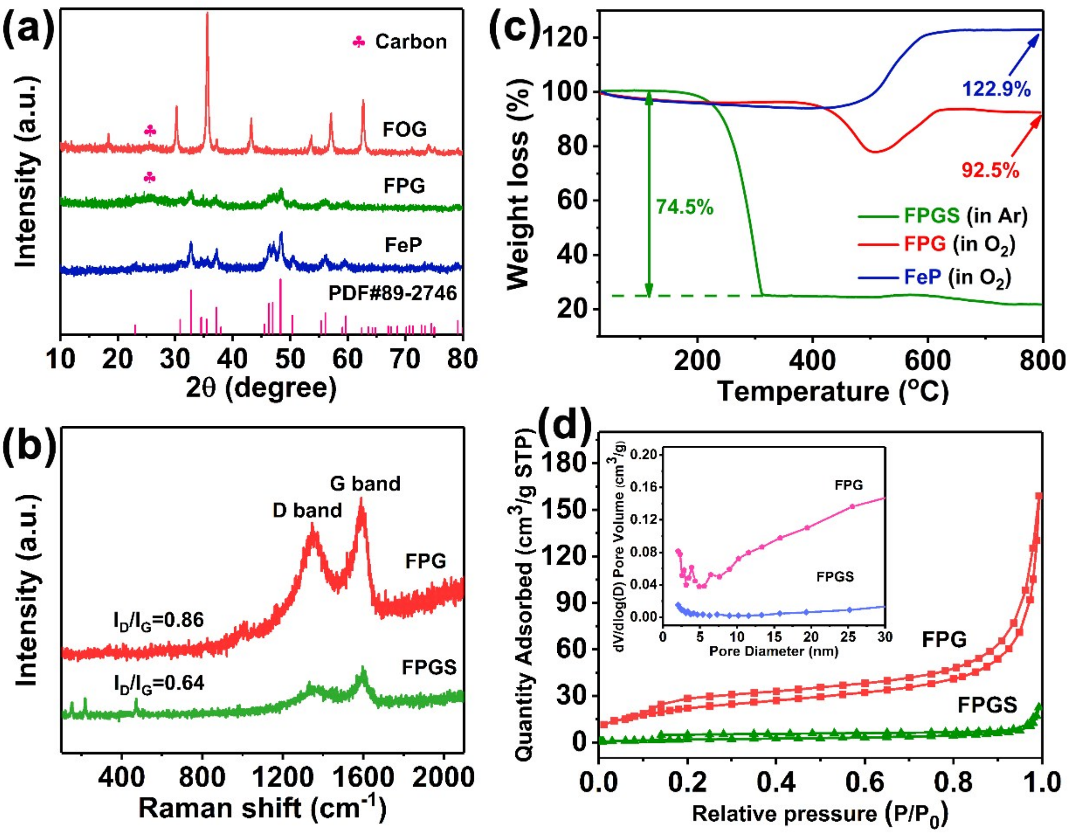

Fig. S3. a) XRD patterns of FOG, FPG and FeP composite. b) Raman spectral of the 3D porous FPG and FPGS composite. c) TGA analysis of FPG, FPGS and FeP composite. d) N_2 adsorption-desorption isotherms and the corresponded pore size distributions of FPG and FPGS.

The TG calculation process:

The carbon content in the FeP/rGO composite can be calculated according to the TGA results as follows: We define the masses of FeP and rGO in the FPG are X_{FeP} and X_{rGO}, respectively. After TGA test, the FeP component increases by 22.9 wt%. While the rGO component was completely burned under O_2 atmosphere, generating a total weight loss of 7.5 wt% of FPG. Thus, according to the follow equation:

$$(X_{FeP} + X_{rGO}) \times (1 - 7.5\%) = X_{FeP} \times (1 + 22.9\%)$$

the ratio of (X_{FeP} : X_{rGO}) is 3.125. Then the rGO content was calculated to be 24.7 wt%.

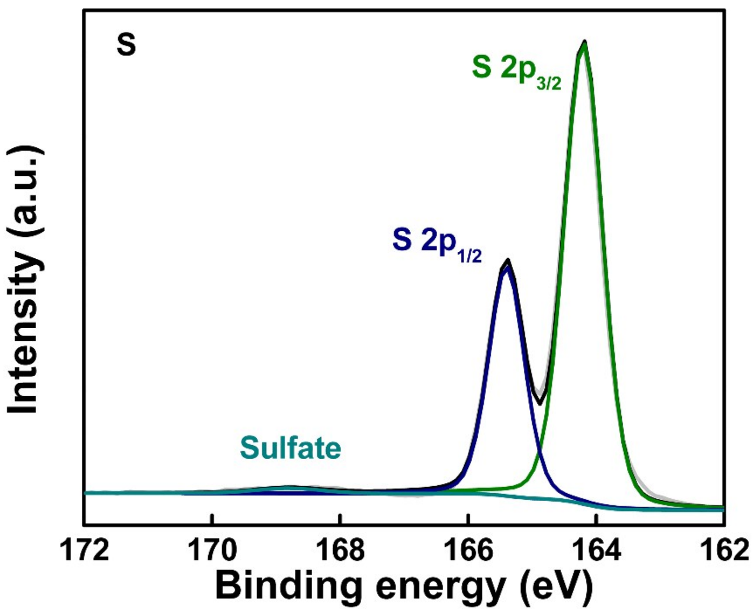

Fig. S4. The XPS high resolution spectrum of pure S.

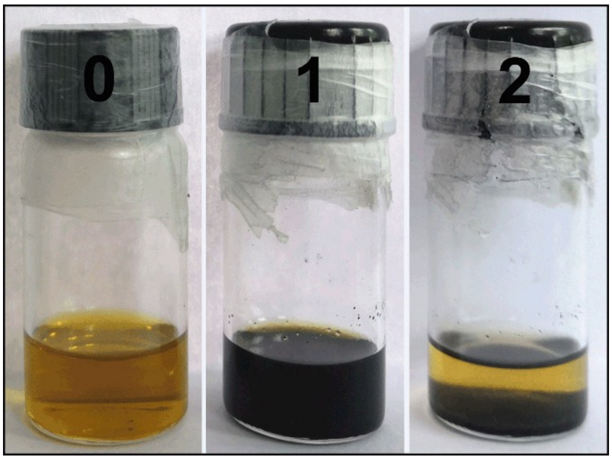

Fig. S5. The photograph of a Li_2S_6 solution before and after the addition of rGO.

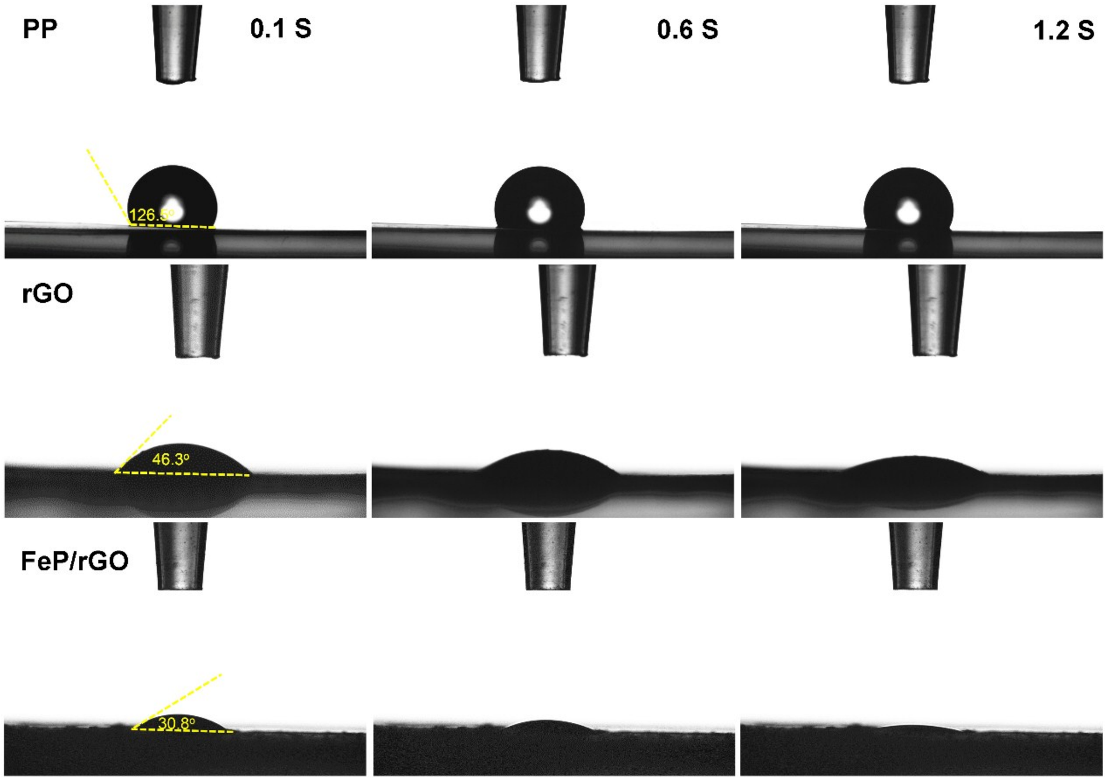

Fig. S6. The water contact angle for PP separator, rGO and FeP/rGO coupling layers.

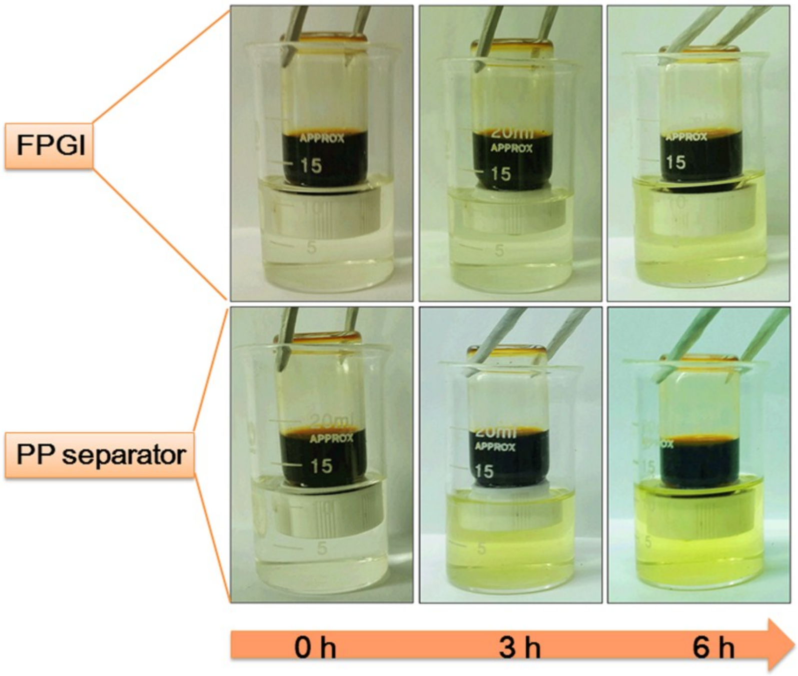

Fig. S7. Polysulfdes permeation measurements with PP separator and the FPGI.

Table S1. Comparison of electrochemical performance of LSBs with different types of separators/interlayers.

Interlayer	Cycle number	Cycling stability	Capacity retention (%)	Capacity decay rate (%)	Ref.
PANI-GO	150	initial capacity 1261 mAh g^{-1}, 896 mAh g^{-1} retained at 0.5 C	73	0.18	1
CoP/KB	200	initial capacity 1068 mAh g^{-1}, 772 mAh g^{-1} retained at 0.5 C	72.3	0.14	2
PAA-SWNT	200	initial capacity 770 mAh g^{-1}, 573 mAh g^{-1} retained at 1 C	74.4	0.12	3
MWCNTs/NC QDs	500	initial capacity 1330 mAh g^{-1}, 650.7 mAh g^{-1} retained at 0.5 C	48.9	0.1	4
Black phosphorus	100	initial capacity 930 mAh g^{-1}, 800 mAh g^{-1} retained at 0.2 C	86.0	0.14	5
Graphene oxide/carbon nanotube	100	initial capacity 1370 mAh g^{-1}, 787 mAh g^{-1} retained at 0.2 C	58.0	0.42	6
WN/CC	500	initial capacity 1337 mAh g^{-1}, 814 mAh g^{-1} retained at 100 mA g^{-1}	60.9	0.078	7
FPGS-FPGI	500	initial capacity 1238 mAh g^{-1}, 925.7 mAh g^{-1} retained at 0.5 C	74.7	0.05	This study

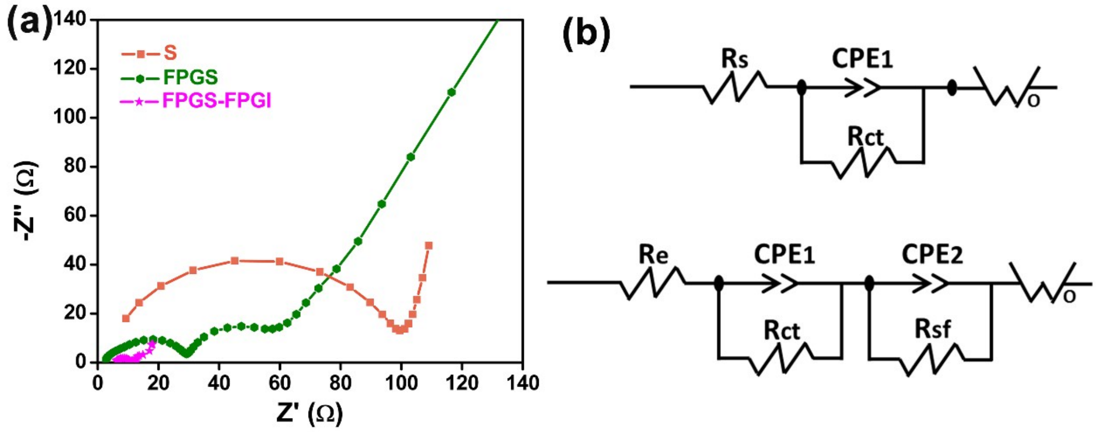

Fig. S8. a) The Nyquist plots of the cells with S, FPGS and FPGS-FPGI after 500 cycles from 100 to 10 mHz at room temperature. b) The corresponding equivalent circuits of the different cells.

Table S2. Fitting results of EIS plots.

cell	R_e/(Ω)	R_{ct}/(Ω)	R_{sf}/(Ω)
FPGS-FPGI	6	3.6	0.6
FPGS	2.4	25	22
S	3.09	89.5	-

Table S3. Summary of D_{Li}^+ at peaks A, B, C for S, FPGS and FPGS-FPGI cell.

Cell	FPGS-FPGI	FPGS	S
D_{Li}^+ at peak A ($cm^2\ s^{-1}$)	1.15×10^{-8}	2.03×10^{-9}	9.58×10^{-11}
D_{Li}^+ at peak B ($cm^2\ s^{-1}$)	4.54×10^{-9}	1.39×10^{-10}	1.98×10^{-11}
D_{Li}^+ at peak C ($cm^2\ s^{-1}$)	2.53×10^{-9}	1.25×10^{-10}	1.23×10^{-11}

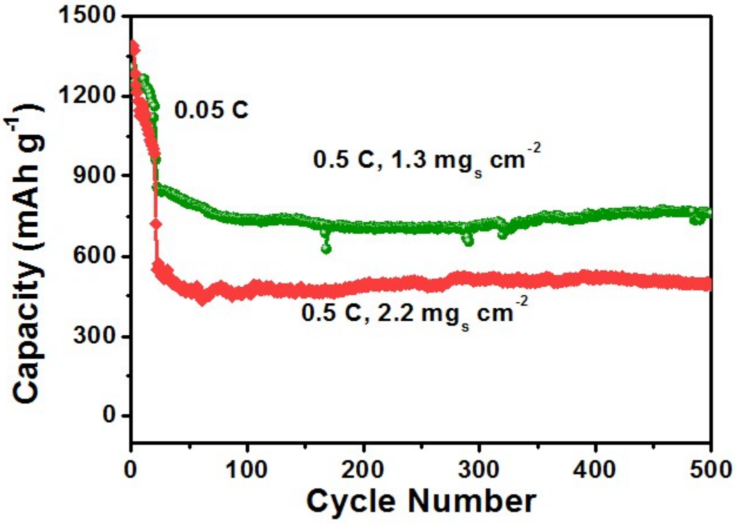

Fig. S9. Cycling performance of the cell of FPGS-FPGI with different sulfur loading.

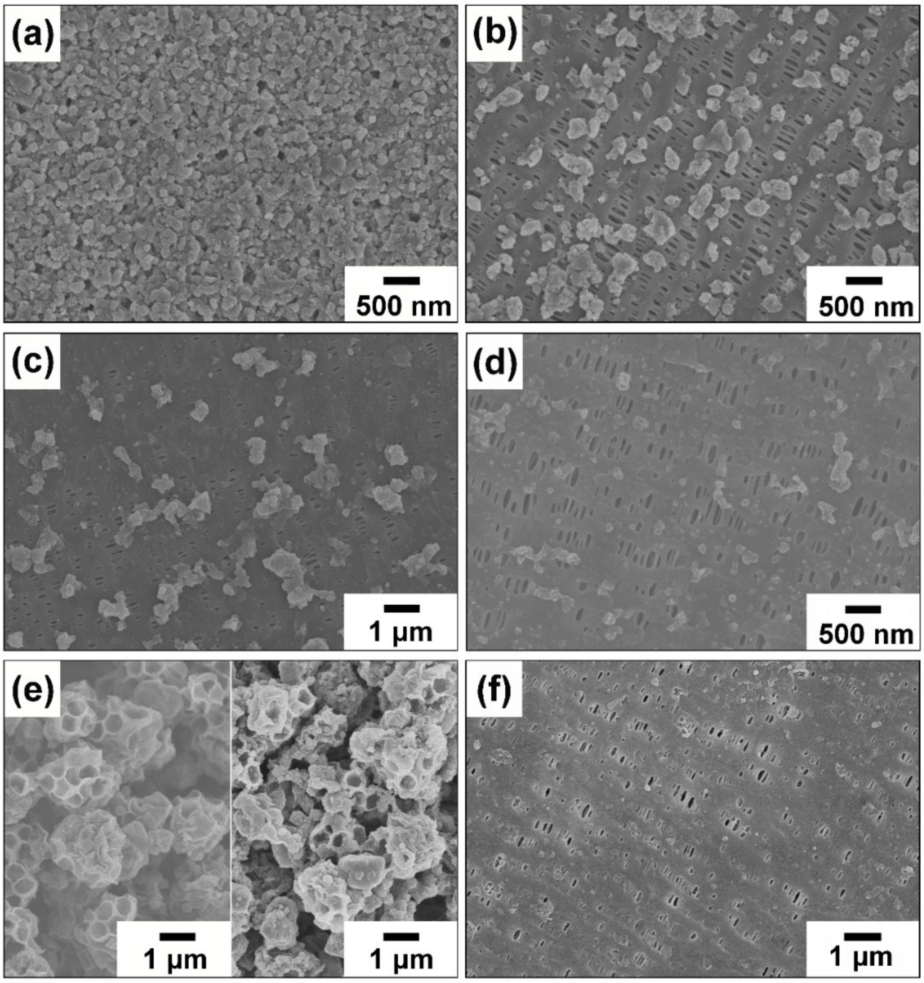

Fig. S10. SEM images of the separator surfaces towards cathode in cells of a) S, c) FPGS and the separator surfaces towards anode in cells of b) S, d) FPGS. e) SEM image of the separator surfaces towards cathode in cell of FPGS-FPGI before and after cycles. f) SEM image of the separator surfaces towards anode in cells of FPGS-FPGI.

Reference

[1] L. X. Yin, H. Dou, A. X. Wang, G. Y. Xu, P. Nie, Z. Chang and X. G. Zhang, *New J. Chem.*, 2018, **42**, 1431-1436.

[2] X. X. Chen, X. Y. Ding, C. S. Wang, Z. Y. Feng, L. Q. Xu, X. Gao, Y. J. Zhai and D. B. Wang, *Nanoscale*, 2018, **10**, 13694-13701.

[3] J. H. Kim, J. Seo, J. Choi, D. Shin, M. Carter, Y. Jeon, C. W. Wang, L. B. Hu and U. Paik, *ACS Appl. Mater. Inter.*, 2016, **8**, 20092-20099.

[4] J. Sun, Y. M. Sun, M. Pasta, G. M. Zhou, Y. Z. Li, W. Liu, F. Xiong and Y. Cui, *Adv. Mater.*, 2016, **28**, 9797-9803.

[5] Y. Pang, J. S. Wei, Y. G. Wang and Y. Y. Xia, Adv. *Energy Mater.*, 2018, **8**, 1702288.

[6] J. Q. Huang, Z. L. Xu, S. Abouali, M. A. Garakani and J. K. Kim, *Carbon*, 2016, **99**, 624-632.

[7] Y. G. Wang, R. J. Luo, Y. G. Zhang, Y. Guo, Y. Lu, X. M. Liu, J. K. Kim and Y. S. Luo, *ACS Appl. Energy Mater.*, 2019, **2**, 3314-3322.